IOSR Journal of Mechanical and Civil Engineering (IOSR-JMCE)
e-ISSN: 2278-1684,p-ISSN: 2320-334X, Volume 13, Issue 6 Ver. V (Nov. - Dec. 2016), PP 18-22
www.iosrjournals.org

Fatigue behavior of a $Fe_{58.12}Nb_{13.74}B_{28.14}$ bulk metallic glass under uniaxial tension-tension loading mode

Gyansah, L[1] and Adetunde, I.A[2]
[2]*Williams V. S. Tubman University, Maryland County, Liberia.*

Abstract: *This paper investigates the fatigue behavior of $Fe_{58.12}$ $Nb_{13.74}B_{28.14}$. Suction mold casting technique was used to fabricate the Fe-based bulk metallic glass. The endurance limit of the Fe-based bulk metallic glass was investigated by using computer-controlled electrohydraulic testing machine, operated at 25 Hz with stress ratio of 0.1., using tension-tension mode. Xrd and dsc experiments were carried out to ascertain whether the material is truly amorphous. The fatigue endurance limit of $Fe_{58.12}Nb_{13.74}$ $B_{28.14}$ was obtained to be approximately 975 MPa for stress range definition. Fractography of the fracture surfaces indicated that there are crack initiation sites.*

Keywords: *bulk metallic glasses, low cycle fatigue, high-cyle fatigue, fractography, fracture surface, S-N curve*

I. Introduction

Fatigue failure has played a significant role in structural analysis. A number of researches have made attempts to understand the influence of fatigue on material integrity. Others have investigated fatigue failure in steels, aluminum and ceramics etc. There have also been advances in fatigue crack growth in materials such as steel and aluminum alloys [1-7]. For instance, L.P. Borrego [8] investigated the fatigue crack growth in heat-treated aluminum alloys. In his research, alloys aged hardened by artificially ageing and simultaneously with a lower content of these alloying elements possessed plasticity-induced closure is dominant.

Recently, there have been research advances in Fe-based bulk metallic glasses (BMGs). These materials possess excellent magnetic properties and good mechanical properties [9–12].

For instance, in based bulk metallic glasses, magnetic properties and glass-forming ability (GFA) are among the most concerned aspects that are needed in industries. Most researchers have tailored their ability to manipulate the mechanical properties such as magnetic and GFA by substitution method [13-20]. For BMG's, many factors could influence fatigue behavior; example, chemical environment, specimen geometry, mean stress, material quality, cyclic frequency and surface condition [21]. Hence, understanding of BMG fatigue mechanism is very limited because of these multiple factors.

This research paper investigated the fatigue behavior of $Fe_{58.12}$ $Nb_{13.74}$ $B_{28.14}$ (BMG) under uniaxial tension-tension mode. The BMG fatigue behavior was characterized with different loading modes. The Fe-based bulk metallic glass was fabricated using the suction mold casting method (arc melting). XRD and DSC tests confirmed that the as-cast material is amorphous. The corresponding S-N curve is also presented. The fracture surfaces were analyzed by scanning electron microscope (SEM).

II. Materials and Methods

2.1.1 Materials Sample Preparation

$Fe_{58.12}$ $Nb_{13.74}$ $B_{28.14}$ bulk metallic glass was used in the experiment. It was fabricated via copper mold cast technology with a mixture of pure iron (Fe), Niobium (Nb) and Boron (B) metals in an argon atmosphere. The as-cast samples had an 8 mm diameter and 80 mm length (Fig.1). The as-cast samples were machined into the un-notched tapered specimens with screw-head to follow ASTM standard before fatigue test. This was to minimize surface effects in the uniaxial fatigue tests. Each specimen was then visually inspected to ensure no surface defects or notches which might cause crack initiation sites. The transverse cross sections of the as-cast samples were studied by X-ray diffractometer with Cu-Kα radiation. Phase transformations during heating were studied by differential scanning calorimetry (DSC-2000) at a heating rate ranging from 20 K/min. X-ray diffraction (XRD) and differential scanning calorimetry (DSC) results confirmed that the metallic grass is fully amorphous (Figs. 4 (a) and (b)). Furthermore, the samples were polished and etched with Nitric acid 40 ml (HNO_3), also known as aqua fortis, 20 ml Hydrofluoric acid (HF), and 40 ml water (H_2O) and examined by electronic optical microscopy to observe if any crystallites were present (Fig.3.). The etched samples were also examined by SEM (Fig.2). However, no crystallites were observed.

Fig. 1. As-cast $Fe_{58.12}Nb_{13.74}B_{28.14}$ **Fig. 2.** SEM view of as-cast sample, no crystalline phases Seen

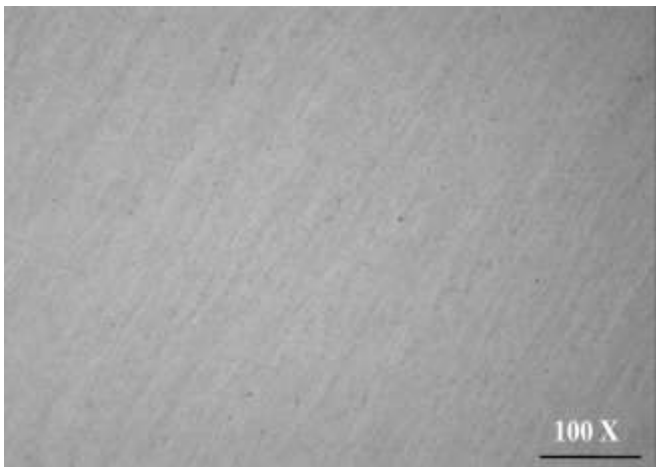

Fig.3. Microscope view of as-cast $Fe_{58.12}Nb_{13.74}B_{28.14}$ showing no crystalline phases

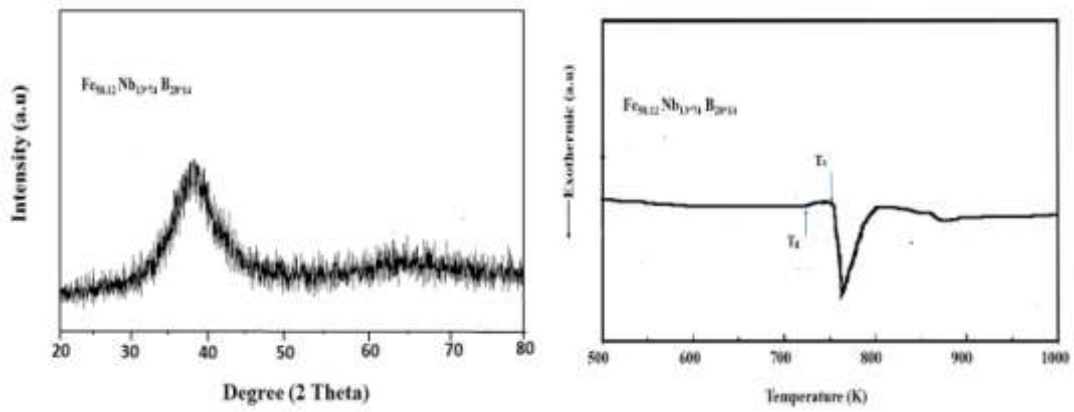

Fig. 4. (a) X-ray diffraction of $Fe_{58.12}Nb_{13.74}B_{28.14}$ showing broad Bragg's peak without crystalline phases (b) DSC curve for the Fe-based bulk metallic grass showing grass transition T_g and crystallization temperature T_x.

III. Fatigue Experiment

Before fatigue test was conducted on the samples, we performed a tension test at a speed of 0.255 mm/min to obtain the tensile strength of the sample to enable computation of fatigue ratio. The value of the tensile strength was approximately 2220 MPa. For fatigue test, samples were tested at stress amplitudes with stress ratio (R), (i.e. $R=\frac{\sigma_{min}}{\sigma_{max}}$), where σ_{min} and σ_{max} denote minimum and maximum stresses for one cyclic loading respectively. The stress ratio was 0.1 and the frequency was 25 Hz. Approximately 10^7 high-cycle fatigue was pre-set for all the fatigue test. Stress-controlled mode was used for the fatigue test. Which

presuppose that all samples tested must fail before the pre-set cycle limit. After failure, samples are assembled for fractography examinations using scanning electron microscopy (model; Supra 35).

IV. Results and Discussion

S-N curve result of the as-cast Fe58.12 Nb13.74 B28.14 is as shown in Fig.5. It could be seen that at approximately 105 cycles to failure, a value of 975 MPa remains appreciably constant. This is indicated by arrow A in Fig.5.Low cycle regime is less than 105 cycles to failure and greater than that is described as high-cycle regime (Fig.5.). If the stress range is higher than 975 MPa, the fatigue live is not stable. The samples fail at a lower cycles to failure (Nf) under the various loading modes. If the stress range is less than 975 MPa, the sample could have run forever without failing. Hence, the fatigue endurance limit under cyclic tension-tension mode was 975 MPa. The fatigue ratio which is defined as ratio of fatigue limit to ultimate tensile strength was 0.44.

What would have contributed to the fatigue endurance limit of 975 MPa? Published papers claimed that the present of strong stress gradients and reduced stress at the crack initiation sites (Fig.6 (a), (b) and (c)) could account for this fatigue limit. However, fatigue life is controlled more by crack propagation than crack initiation. But, the as-cast samples had a small stress gradient instead of stress concentration, hence it will be very difficult for stress concentration to be accounted in this result. It could also be seen that the samples fractured with a maximum radius between 0.4 to 0.8 mm depending on the loading condition. The radius value where the fracture occurred was approximately 0.6 mm, meaning the stress at the fatigue initiation site was almost equal to the nominal stress (Fig.6 (a), (b) and (c)). Hence, the result discrepancy under different loading modes had little or nothing to do with reduced stress at the fatigue initiation site. The relationship between the fatigue limit (σa) and cycles to failure can be derived by plotting the values above fatigue limit with cycles to failure (Nf). That will yield a linear equation in the form:

$$\sigma_a = 4876.5 - 981.2(N_f) \qquad \text{(a)}$$

The equation was found to fit the data with a correlation coefficient of 0.96. The intercept on the vertical axis is 4876.5 MPa. Fractography of the fractured surfaces of the samples revealed three regions: the fatigue-crack initiation, crack propagation and final fractured site. The crack initiation sites are illustrated with black arrows, the final fractured area is indicated by the red circles and between the crack initiation sites and the final fractured surface is what we named as crack propagation (Fig.6 (a), (b) and (c)). It was observed that crack initiation sites where more profound at higher cyclic stresses than lower cyclic stresses (Fig.6 (a) and (b). Two kinds of crack initiation mechanisms in bulk metallic glasses are known. (1) Shear banding and (2) Intrusive defects. In shear banding mechanism, higher cycle stresses caused the sample to fail below yield strength promoting shear bands propagation on the tensile surface due to cyclic softening. From that state, final shear band openings in the BMG's lead to microcrack formation given birth to crack initiation. Material defect is also another fatigue crack initiation mechanism. At higher cycle stresses, fatigue crack initiates from inhomogeneities, however, it has little effect on fatigue endurance limit because it is mainly controlled by crack propagation in low cyclic stresses regime. Regardless of the crack initiating from the shear bands or defects, fatigue endurance limit was observed to be approximately 975 MPa. The microcrack initiation was evidenced at cyclic stresses above 975 MPa. Once the microcrack is formed, it propagated quickly to failure (Fig.6 (a), (b) and (c)). For the specimens under uniaxial tension-tension loading, when the applied stress was too low to form a microcrack from the shear bands or some large defect on the surface, the crack initiation shifted to another place which was relatively weaker than the perfect amorphous matrix and needed more crack initiation time. As for cyclic microcrack propagation in BMGs, the mechanism could be related to the blunting and re-sharpening of the crack tip while the necessary plastic flow alternately to blunt and sharpen the crack tip occurred by limited shear band at crack tip. The change of initiation site was similar with the high-cycle fatigue and ultrahighcycle fatigue regime in crystalline materials.

Fig. 6(d) shows the enlarged view of final fractured site sample surface at a lower cyclic stresses of 995 MPa. The surface resembles a group of irregular particles. Based on the appearance of these particle sheets, the interfaces along the surfaces of the sheets were weak and facilitated crack initiation and propagation. At a stress level above 975 MPa, the shear bands were also a determined mechanism for crack initiation. In general, the fatigue cracks grow unimpeded once initiated because of lack of microstructural barriers in BMG'S.
The un-notched round samples employed in the current work exhibited a much higher endurance limit.

The as-cast BMGs always consist of many defects such as porosity, inclusion, and other imperfect amorphous phase. At a higher stress level, the defects may have little influence on the crack initiations but not the case at a lower stress level in high cycle fatigue range. Whatever the mechanisms were, once the crack initiation was formed it propagated fast to failure The total fatigue life was controlled by crack initiation instead of crack propagation at lower stress level in high cycle fatigue range with a change of the crack initiation site from surface to interior under uniaxial TT loading mode. The total life may be mainly determined by crack propagation despite of the high crack growth rate and low threshold intensity range in low cycle fatigue range,

because the stress was so high that the crack could initiate from shear bands easily, but not necessary from the defects in material. Thus, the defects have little effect on the crack initiation compared with that in high cycle fatigue mechanism.
The fatigue properties must have a larger improvement if the defects in the BMGs decrease.

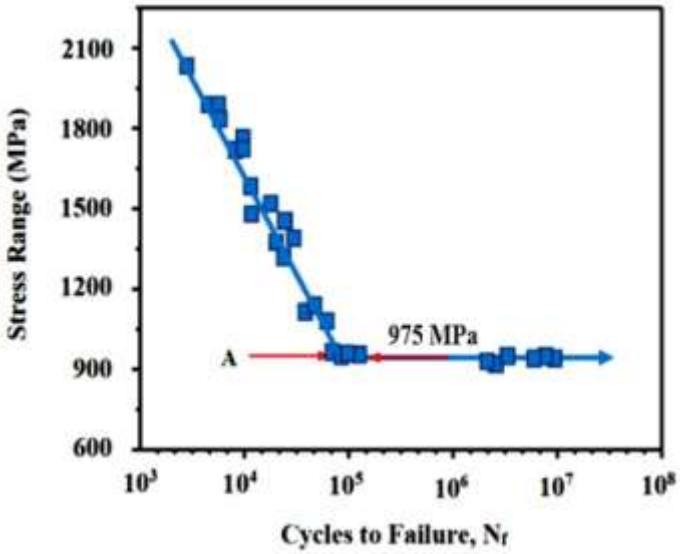

Fig. 5. S-N curve under uniaxial tension-tension loading mode

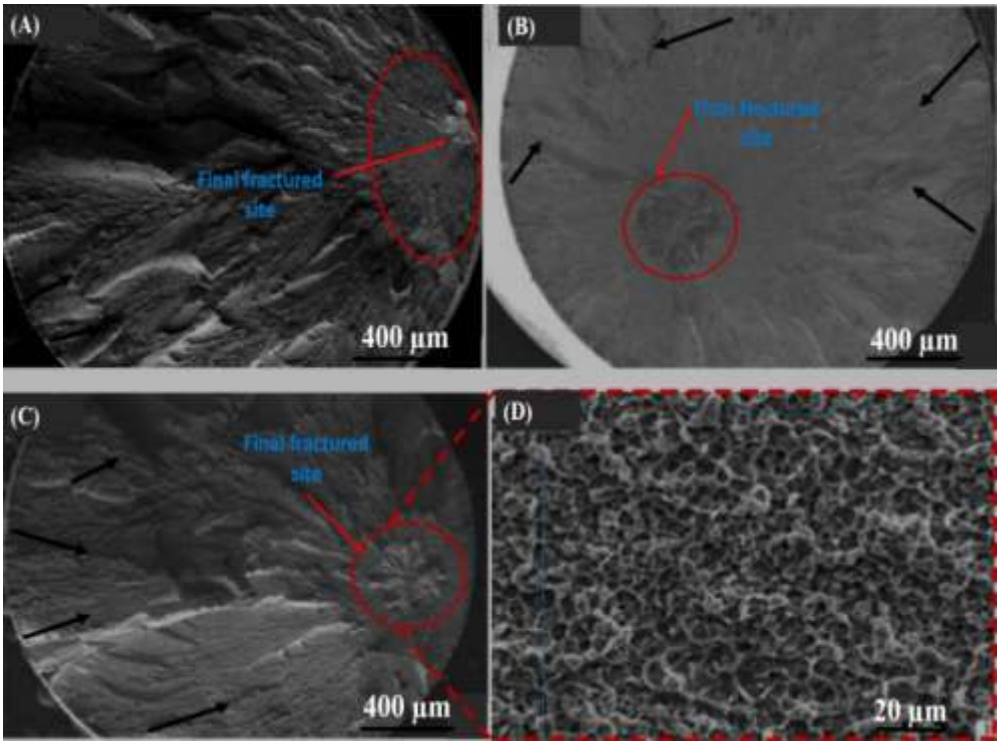

Fig. 6. (a), (b) and (c) indicate initiation location on the fractured surface cycled at 1900 MPa, 1300 MPa, and 995 MPa respectively (d) the detailed morphology of the final fractured site .

V. Conclusion

- Fatigue behavior of $Fe_{58.12}Nb_{13.74}B_{28.}$ has been studied. The fatigue endurance limit was observed to be 975 MPa under uniaxial tension-tension mode. The engineering equation fitting the behaviour above fatigue limit was proposed to $\sigma_a = 4876.5 - 981.2(N_f)$ (uniaxial tension-tension mode). Fractography of the fractured surfaces indicated that there are crack initiation and final fractured sites. At higher cyclic stresses

greater than 975 MPa, cracks are caused by both shear banding or material defect and the fatigue life was controlled by crack propagation till failure.

VI. Recommendations

Fatigue behavior for a Fe-based bulk metallic glass (BMG) notched specimen should be investigated.

Acknowledgement

Authors wish to acknowledge the support of William V.S. Tubman University, Liberia.

References

[1]. Aziz Egemen VARLI and Rıza G¨URB¨UZ, (2006), Fatigue Crack Growth Behaviour of 6013 Aluminium Alloy at Different Ageing Conditions in Two Orientations, Turkish J. Eng. Env. Sci. 30 (2006) 381 – 386.
[2]. Williams, J.C. and Starke Jr., E.A., "Progress in Structural Materials for Aerospace Systems", Acta Materialia, 51, 5775-5799, 2003.
[3]. Gurbuz, R. and Sarıoglu F., "Fatigue crack growth behaviour in aluminium alloy 7475 under different aging conditions", Materials Science and Technology, 17, 1539-1543, 2001.
[4]. Biallas, G., Alléhaux, D., Marie, F., Role of residual stresses on Fatigue Crack Propagation of FSW 6056-T78 aluminium joints under various technologies, Materials Science Forum Vols. 519-521, pp. 1089-1094, 2006.
[5]. Dugdale, D.S. (1960). Yielding of steel sheets containing slits. Journal of the Mechanics and Physics of Solids 8,
[6]. 100–104.
[7]. H. J. Cialone and J. H. Holbrook, Effects of gaseous hydrogen on fatigue crack growth in pipeline steel. Metallurgical Transactions A 1984;16 A (1):115-122.
[8]. A. Suresh and R. O. Ritchie, Mechanistic dissimilarities between environmentally influenced fatigue-crack propagation at near-threshold and higher growth rates in lower strength steels. Metal Science 1982; 16:529-538.
[9]. L.P. Borrego a,*, J.M. Costa b, F.V. Antunes b, J.M. Ferreira b, (2009) Fatigue crack growth in heat-treated aluminium alloys, Engineering Failure Analysis, elservier, PP.2-8.
[10]. Q. Li, J.F. Li, P. Gong, K.F. Yao, J.G. Gao, H.X. Li, Formation of bulk magnetic ternary $Fe_{80}P1_3C_7$ glassy alloy, Intermetallics 26 (2012) 62–65.
[11]. Z.P. Lu, C.T. Liu, W.D. Porter, Role of yttrium in glass formation of Fe-based bulk metallic glasses, Appl. Phys. Lett. 83 (2003) 2581–2583.
[12]. W.M. Yang, H.S. Liu, X.D. Fan, L. Xue, C.C. Dun, B.L. Shen, Enhanced glass forming ability of Fe-based amorphous alloys with minor Cu addition, J. Non-Cryst. Solids 419 (2015) 65–68.
[13]. J.H. Zhang, C.T. Chang, A.D. Wang, B.L. Shen, Development of quaternary Fe based bulk metallic glasses with high saturation magnetization above 1.6 T, J. Non-Cryst. Solids 358 (2012) 1443–1446.
[14]. B.L. Shen, C.T. Chang, Enhancement of glass-forming ability of FeCoNiBSiNb bulk glassy alloys with superhigh strength and good soft-magnetic properties, J. Appl. Phys. 102 (2007) 023515.
[15]. W.M. Yang, H.S. Liu, X.D. Fan, L. Xue, C.C. Dun, B.L. Shen, Enhanced glass forming ability of Fe-based amorphous alloys with minor Cu addition, J. Non-Cryst. Solids 419 (2015) 65–68.
[16]. H.Y. Jung, S. Yi, Enhanced glass forming ability and soft magnetic properties through an optimum Nb addition to a Fe-C–Si–B–P bulk metallic glass, Intermetallics 18 (2010) 1936–1940.
[17]. Wang GY, Liaw PK, Peker A, Yang B, Benson ML, Yuan W, et al. Fatigue behavior of ZreTieNieCueBe bulk-metallic glasses. Intermetallics 2005;13: 429e35.
[18]. Z.B. Jiao, H.X. Li, J.E. Gao, Y. Wu, Z.P. Lu, Effects of alloying elements on glass formation, mechanical and soft-magnetic properties of Fe-based metallic glasses, Intermetallics 19 (2011) 1502–1508.
[19]. J.W. Li,W.M. Yang, D. Estéves, G.X. Chen,W.G. Zhao, Q.K. Man, Y.Y. Zhao, Z.D. Zhang, B.L. Shen, Thermal stability, magnetic and mechanical properties of Fe–Dy–B–Nb bulk metallic glasses with high glass-forming ability, Intermetallics 46 (2014) 85–90.
[20]. Y.J. Huang, J. Shen, J.F. Sun, X.B. Yu, A new TieZreHfeCueNieSieSn bulk amorphous alloy with high glass-forming ability, J. Alloy Compd. 427 (2007) 171e175.
[21]. L. Huang, C. Pu, R.K. Fisher, D. Mountain, P.K. Liaw, W. He, A Zr-based bulk metallic glass for future stent applications: materials properties, finite element modeling, and in vitro human vascular cell response, Acta Biomater. 25 (2015) 356e368.
[22]. Tsai PH, Li JB, Chang YZ, Lin HC, Jang JSC, Chu JP, et al. Fatigue properties improvement of high-strength aluminum alloy by using a ZrCu-based metallic glass thin film coating. Thin Solid Films 2014;561:2832.